Ultrafast tomography experiment setup at D-1 Beamline at CHESS

The experiment setup consists of three major parts: x-ray source, injection chamber, and detector, as shown schematically in Fig. EPAPS1a. The x-ray beam produced by synchrotron radiation is monochromatized to 6.0 keV with an energy bandwidth ($\Delta E / E$) of about 1% using a double-multilayer monochromator. The wide bandwidth ensures a high beam intensity required for microsecond (μs) imaging. This x-ray energy is optimal for probing the fuel, a blend of a calibration fluid and a cerium-containing fuel additive (to be described later). The monochromatized x-ray beam is collimated to 15 mm (horizontal, H) × 2 mm (vertical, V) by a set of slits as shown in Fig. EPAPS1a. The higher-order harmonic contamination (at 12 keV, 18 keV, etc.) was rejected by a flat palladium-coated mirror (not shown in the figure) positioned after the slits.

The next important component in the tomography setup is a cylindrical spray chamber that is made of stainless steel with 11-cm inner diameter and 21-cm height. This injection chamber is intended to provide an environment enclosure for the fuel sprays. As shown in Fig. EPAPS1a, there are two identical x-ray transparent windows situated symmetrically on the chamber with a 120° x-ray viewing angle. The windows are 6.5 cm high and are covered with polymer thin films. The injection nozzle is mounted on top of the chamber, as shown in Fig. EPAPS1a. The nozzle has an outwardly opening pintle and an annular orifice with a diameter of 1.9 mm. The injection pressure is about 7 MPa, and the nominal duration of the spray is 1 ms. Also fit to the chamber are two inlets and one outlet for flowing nitrogen gas through the chamber to scavenge the fuel vapor. On the side of the chamber, there is also a fuel drain line. The environment in the spray chamber is maintained at one atmospheric pressure and at room temperature (27-30°C in the D-1 radiation enclosure). The spray chamber is designed to rotate and to translate in precise steps, while the x-ray source and the detector are stationary. In this system, we use a horizontal rotational stage and a vertical translational stage to rotate the spray chamber and to select the slice to be

imaged in the vertical direction. The minimum rotation angle is 0.0025°, and the minimum step size for the translation stage is 1.27 μm. In the experiment, the parallel x-ray beams penetrate the spray at a given view angle θ, and, after completion of the scans in temporal steps, the injector nozzle rotates a small angle Δθ, and the temporal scans are repeated. This process is continued until the completion of a 180° rotation is completed. The rotating injection nozzle in this tomography system poses a rigorous requirement of alignment. First, the rotation axis and the x-ray beam should be orthogonal, which is achieved by adjusting the optical table supporting the spray chamber. Second, it is essential to ensure the coincidence of the rotation axis and the center of the injection nozzle. The alignment is completed by adjusting the X-Y translation stages mounted under the spray chamber (not shown in the schematic). All the rotational and translational stages are motorized.

Another key component in the setup is the ultrafast x-ray framing detector – PAD. The pixel size of the PAD is 150×150 μm^2. The single imaging area is 92 (H) × 31 (V) pixels limited by the x-ray beam size. The complete imaging area is built up by shifting the position of the injector relative to the beam and the PAD. During the experiment, the spray is fired at 1.15 Hz, and a series of frames is taken at various delay times. The exposure time per frame is set to 5.13 μs (twice the CHESS synchrotron period) with an interval between frames of 15.38 μs. Each image is obtained by averaging 20 fuel-injection cycles. The total acquisition time for each angle is about 5 minutes.

The fuel used in this study was a blend of a calibration fluid and a cerium additive (concentration of 4%). The cerium additive enhances the absorption by about 50%. The calibration fluid is a simulated fuel with properties similar to gasoline with precisely controlled viscosity and specific gravity specifications. With the choice of the x-ray photon energy and the line-of-sight transmission geometry, the dominant interaction between the x-rays and the fuel spray is absorption, rather than scattering-based phase-contrast mechanism as in our previous work (*1*).

Rotation axis **Translation direction**
Injector
X-ray window **N$_2$ flow inlet**
X-Y slits

PAD

6 keV x-ray beam

N$_2$ flow outlet **Spray Chamber**
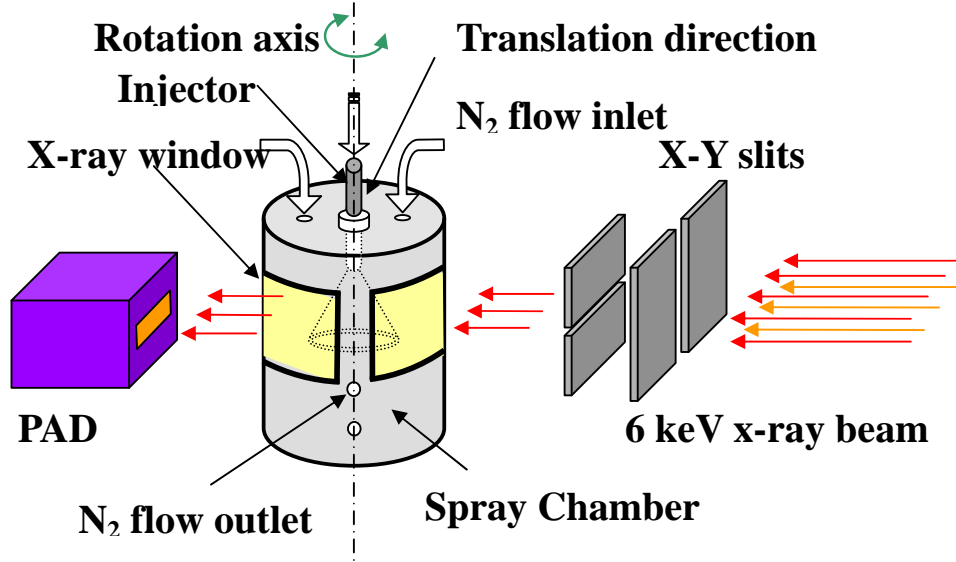
Fig. EPAPS1a. Schematic of experiment setup.

Tomography reconstruction and spatial resolution

As illustrated in our previous work (*2*), the mathematical description of the fuel spray tomography is built upon the geometry described in the previous section. Consider parallel x-ray beams penetrate an object (a hollow cone spray in this case) as shown in Fig. EPAPS1b. The function $f(x, y)$ represents the linear attenuation coefficients where (x, y) are Cartesian coordinates defined over one slice of the spray. The other coordinate is (r, s), which is fixed while (x, y) rotates. The spray (i.e., the spray chamber) makes an angle θ with the r axis. The two coordinate systems can be transformed mutually by the following formula,

$$\begin{bmatrix} x \\ y \end{bmatrix} = \begin{bmatrix} \cos\theta & \sin\theta \\ -\sin\theta & \cos\theta \end{bmatrix} \begin{bmatrix} r \\ s \end{bmatrix}. \tag{1}$$
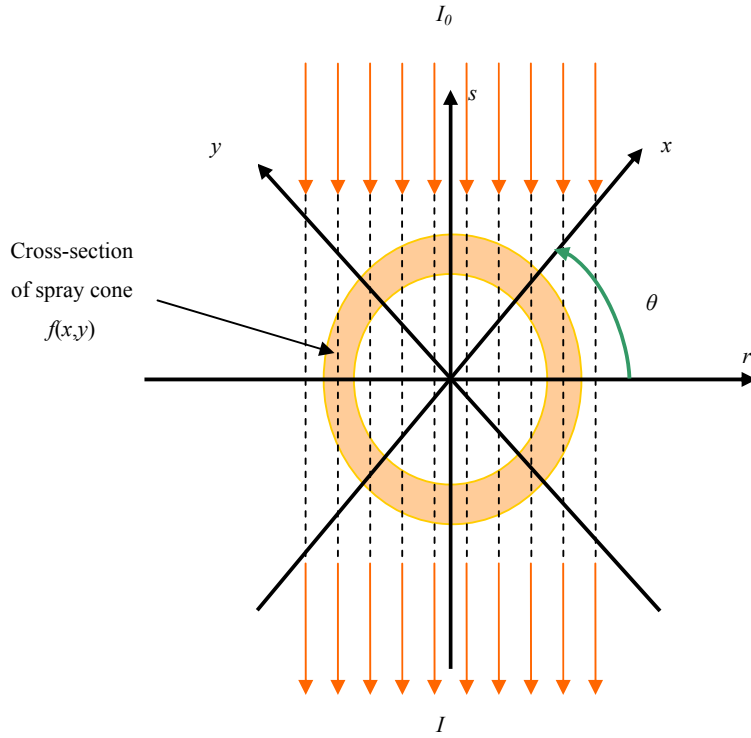
Fig. EPAPS1b. Parallel x-ray beam penetrating spray cone and coordinate systems.

Thanks to the monochromatic x-ray beam, the intensity profile I as a function of r at given angle θ is simply described by

$$
\begin{aligned}
I(r,\theta) &= I_0 \exp[-\int_s f(x,y)ds] \\
&= I_0 \exp[-\int_s f(r\cos\theta + s\sin\theta, -r\sin\theta + s\cos\theta)ds],
\end{aligned}
\tag{2}
$$

where I_0 is the incident x-ray beam intensity, and Δs *(or ds)* is the spatial interval along the beam path. Then, the sinogram $p(r, \theta)$ is defined by

$$
\begin{aligned}
p(r,\theta) &= -\ln\frac{I(r,\theta)}{I_0} \\
&= \int_s f(r\cos\theta + \sin\theta, -r\sin\theta + s\cos\theta)ds.
\end{aligned}
\tag{3}
$$

The above equation is the mathematical description of the data set recorded by the PAD.

With the sinogram, we can reconstruct $f(x, y)$ by several methods, such as the filtered backprojection (FBP) method, the algebraic reconstruction method, and the Fourier transform method. The algebraic reconstruction method is the slowest algorithm of the three, but it can be used as an online updating method where the projections are not uniformly distributed over $180°$. The results given by the FBP and the Fourier transform methods are very close for our case, but the latter is currently the most efficient algorithm. Thus, we choose the Fourier transform method as our reconstruction method. With the well-known central slice theorem (CST), one can reconstruct $f(x, y)$ through the Fourier transform and the inverse Fourier transform as

$$f(x, y) = F^{-1}\{F[f(x, y)]\} = F^{-1}\{F[p(r, \theta)]\}, \tag{4}$$

where F and F^{-1} are the Fourier transform and the inverse Fourier transform, respectively. The mass density distribution $\rho(x, y)$ is simply derived by

$$\rho(x, y) = \frac{f(x, y)}{\mu_M}, \tag{5}$$

where μ_M is the mass attenuation coefficient of the fuel, which is evaluated through a calibration procedure.

There is one question left to resolve–the number of view angles, which should be determined by considering the reconstruction resolution and the experimental time as well. Obviously, the number of view angles is dependent on the size of the viewing area. A larger viewing area needs more view angles. By equating the radial resolution and the worst-case azimuthal resolution, the minimum number of view angles required is estimated by the following (*3*)

$$N_v = \frac{\pi}{2} N_p, \tag{6}$$

where N_v is the number of view angles, and N_p is the number of pixels. For example, if there are 92 pixels horizontally to record the projections in the PAD, then the minimum N_v is 145. In the actual experiment, 180 view angles are used, which results in about 20 hours scanning time for one cross section.

We note that the most reliable method to determine the spatial resolution of our experiment is to measure a known object, such as a line-pair phantom. However, without having included such a measurement in the experiment, we made our best estimate to determine the reconstruction spatial resolution by considering factors that included angular sampling, data noise, and transform artifacts. First, as discussed above, the 180 angular projections are sufficient for reconstruction without degrading the reconstruction spatial resolution. Second, with the high-intensity synchrotron x-ray beam and multi-shot averaging, our data signal-to-noise ratio (SNR) is better than 100 and well above the required SNR (~5, i.e., Rose's criteria). Such an SNR value ensures a reliable reconstruction and would not introduce additional resolution degradation during the reconstruction process. The results shown in Figure 3 (agreement between the sinograms from the data and reconstruction) also demonstrate the goodness of the reconstruction. Third, we used the direct inverse Fourier transform reconstruction method, which mathematically gives the exact value of the linear attenuation coefficient in each pixel. It may introduce numerical errors, but as shown in Figure 3, the reconstruction is reliable and robust. The reconstruction artifacts are not observed and can be negligible. Lastly, the x-ray beam from synchrotron can be considered as a parallel beam with horizontal or transverse divergence of several milliradians while the source-to-sample and sample-to-detector distances are 15 m and 0.1 m, respectively. There is no distortion caused by a penumbra effect. In addition, the PAD directly detects x-rays without a scintillator or other light-converting media. The point-spread function of the detector is confined in 1 pixel. Therefore, it is reasonable to state that the 150 μm pixel determines the data spatial resolution and reconstruction resolution to be 150 μm, as determined by the detector resolution.

1. Y.J. Wang, X. Liu, K.S. Im, W.K. Lee, J. Wang, K.F. Fezzaa, D.L.S. Hung, J.R. Winkelman, *Nature Physics*, 4, 305-309 (2008).
2. X. Liu, J. Liu, X Li, S. Cheong, D. Shu, J. Wang, M.W. Tate, A. Ercan, D.R. Schuette, M.J. Renzi, A. Woll, S.M. Gruner, Developments in X-ray Tomography IV,

Proceedings of SPIE, Vol. 5535, 21-28 (2004).

3. A.C. Kak, and M. Slaney, *Principles of Computed Tomographic Imaging*, IEEE Press, New York (1999).